

# Surface diffusion: defining a new critical effective radius for holes in thin films

Anna Zigelman<sup>1,2</sup> and Amy Novick-Cohen<sup>1\*</sup>

<sup>1</sup>Department of Mathematics, Technion-IIT, Haifa, Israel

<sup>2</sup>Faculty of Mechanical Engineering, Technion-IIT, Haifa, Israel

\*amync@technion.ac.il

## Abstract

We explore a specific small geometry containing a single thin bounded grain on a substrate with a hole at its center. By employing a mathematical model based on surface diffusion, no flux boundary conditions, and prescribed contact angles, we study the evolution of the hole as well as the exterior surface of the grain, based on energetic considerations and dynamic simulations. Our results regarding the formation and evolution of holes in thin films in small geometries shed light on various nonlinear phenomena associated with wetting and dewetting.

**Keywords:** surface diffusion, thin film stability, wetting and dewetting, hole and hillock formation.

## 1. Introduction

The stability of thin films is critical in innumerable industrial applications [1, 7], and accordingly it has attracted considerable attention in terms of basic research as well [3, 10, 11, 12, 13]. Thin film stability is associated with wetting, dewetting, and hole formation, as well as with numerous more specific experimentally observed phenomena, such as blister formation and rupture, void formation, ligament formation and propagation, hillock formation and rim propagation, [5, 6, 9]. Numerous works have proposed criteria for the stability of holes in thin films in terms of a critical radius, notably e.g. [10, 13].

## 2. The model

Let us consider an axi-symmetric grain that lies on a substrate and is bounded along its sides by a finite radius semi-infinite inert cylinder. The exterior surface of the grain meets the substrate with contact angle  $\alpha \in (0, \pi)$  and normally intersects the bounding cylinder. In what follows all spatial variables were normalized by the radius of the cylinder,  $l$ , and all temporal variables were normalized by  $l^4/B$ , where  $B$  is the Mullins coefficient for surface diffusion [8]. For a 3D view and a meridian cross-sectional sketch of the geometry, see Fig. 1. We assume that the exterior surface evolves by (dimensionless) isotropic surface diffusion,



$$\mathbf{V}_n = -\Delta_S \kappa, \quad (1)$$

where  $\mathbf{V}_n$  denotes the normal velocity,  $\mathbf{n}$  is an outward unit normal,  $\kappa$  is the mean curvature of the surface,  $\Delta_S$  is the surface Laplacian. For simplicity, additional physical effects, such as elasticity or anisotropy, have been neglected. We further assume no flux boundary conditions at the substrate and at the inert wall, namely that  $[\vec{\tau} \cdot \nabla_S \kappa]_{\text{boundary}} = 0$ , where  $\vec{\tau}$  denotes a unit conormal vector to the exterior surface at the boundary and  $\nabla_S$  denotes the surface gradient operator.

The steady states of (1), subject to the no flux boundary conditions, satisfy

$$\kappa = C, \quad C \in \mathbb{R}.$$

Assuming axi-symmetry, the set of such surfaces, (*Delaunay surfaces* after Delaunay, 1841 [2]), are: planes, spheres, catenoids, unduloids, and nodoids. In the context of the present problem, the steady states are nodoids with (constant) negative mean curvature  $C = \lambda < 0$ , where  $\lambda$  is determined by the contact angle and the grain volume.

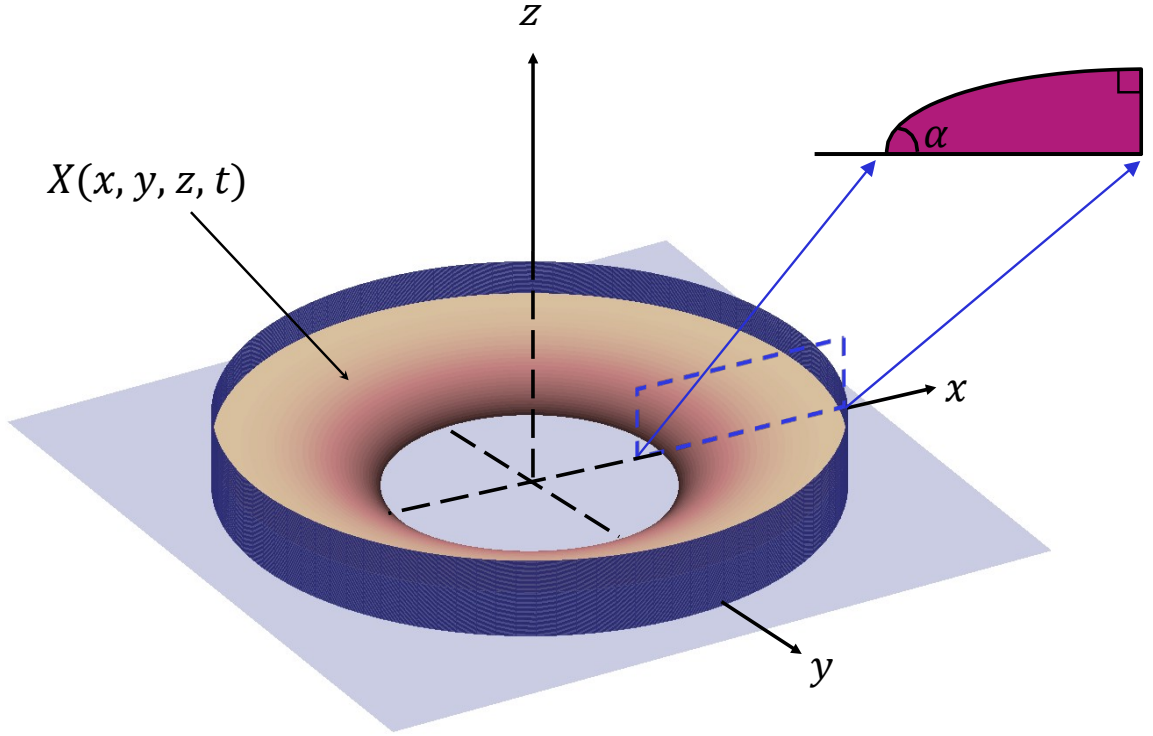


Figure 1: Sketch of an annular axi-symmetric grain, which lies on a substrate and is bounded by an inert cylinder. The exterior surface of the grain normally intersects the bounding cylinder and intersects the substrate with contact angle  $\alpha$ . The meridian cross-sectional profile of the grain is indicated in maroon.

### 3. Results

#### 3.1 Energetic stability

The surface diffusion problem formulated above constitutes  $H^{-1}$  gradient flow [4] for the energy,  $E(t)$ ,

$$E(t) := A_{\text{ex}}(t) + \left( \gamma_{\text{gas}} / \gamma_{\text{ex}} \right) A_{\text{gas}}(t) + \left( \gamma_{\text{grs}} / \gamma_{\text{ex}} \right) A_{\text{grs}}(t), \quad (2)$$

where  $\gamma_{\text{ex}}$ ,  $\gamma_{\text{gas}}$ , and  $\gamma_{\text{grs}}$  denote the surface free energy of the exterior surface, of the hole on the

substrate which is exposed to gas or vacuum, and of substrate which is covered by the grain, respectively, and  $A_{\text{ex}}(t)$ ,  $A_{\text{gas}}(t)$ , and  $A_{\text{grs}}(t)$  denote the corresponding surface areas. The energy  $E(t)$  decreases (is non-increasing) during the evolution, while the grain volume is conserved [4, 15]. The critical points of the energy which satisfy the angle boundary conditions correspond to the set of steady states of our problem. Of interest is to identify the possible steady states, and to order them in accordance with their energy.

For  $\alpha \in (0, \pi)$ , the possible steady states, which correspond to nodoidal surfaces with constant and negative mean curvature, may be expressed via elliptic integrals and parametrized by their mean curvature,  $\lambda$  [4, 15]. In Fig. 2(a), we show the volumes of the nodoidal steady states as functions of the mean curvature,  $\lambda < 0$ , for a set of contact angles,  $\alpha \in (0, \pi)$ . The different colored curves in the figure correspond to different values of the contact angle. These results led us to formulate the following claim [4, 15]:

*Claim 1:* For  $\alpha \in (0, \pi)$  there is a function  $V_{\text{max}}(\alpha) > 0$ , such that for any contact angle  $\alpha \in (0, \pi)$  and for any grain volume  $V \in (0, \infty)$ , if  $0 < V < V_{\text{max}}(\alpha)$  there exist precisely two steady states, if  $V = V_{\text{max}}(\alpha)$  there exists precisely one steady state, and if  $V > V_{\text{max}}(\alpha)$  then no steady states exist.

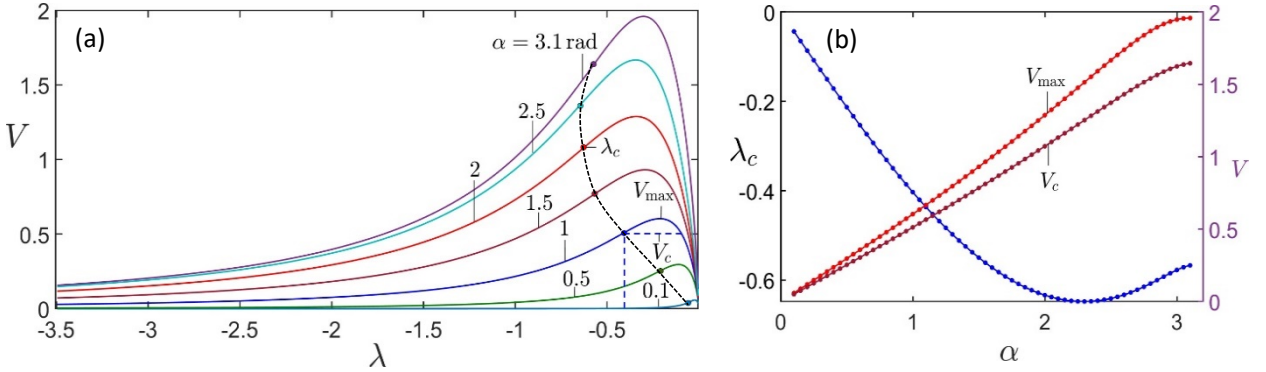


Figure 2: (a) Volume,  $V$ , versus mean curvature,  $\lambda$ , of the steady states for various values of the contact angle,  $\alpha \in (0, \pi)$ . The critical mean curvatures,  $\lambda_c(\alpha)$ , are indicated along each of the  $\alpha$  curves, and for  $\alpha = 1$  rad the maximal,  $V_{\text{max}}$ , and the critical,  $V_c$  are also marked. (b) Critical mean curvature,  $\lambda_c$ , maximal volume,  $V_{\text{max}}$ , and critical volume,  $V_c$ , versus  $\alpha$ .

More specifically when  $V \in (0, V_{\text{max}})$ , according to Claim 1 there is a pair of steady state solutions with the same contact angle,  $\alpha$ , and volume,  $V$ ; one of the pair of steady states, which is to the left in Fig. 2(a) and we will denote by L, has smaller mean curvature and the other steady state, which is to the right in Fig. 2(a) and we will denote by R, has larger mean curvature. We remark that though Claim 1 characterizes the set of steady states and while off-hand one expects the energy of the system to decrease while the solution evolves towards one of the steady states, there may be minimizing sequences leading to closure of the hole. Note that the resulting flat configuration which no longer contains a hole, no longer satisfies the contact angle boundary conditions; hence it is not strictly speaking a steady state for the problem which we described above, consisting of Eqn. (1) and the no-flux and prescribed angle boundary conditions. To gain insight into the limiting evolution, we evaluated the respective energies,  $E_L$  and  $E_R$ , of the steady states L and R, as well as the energy  $E_{\text{flat}}$  of the flat configuration. We conjecture that for initial conditions satisfying the boundary conditions with volume greater than  $V_{\text{max}}$ , the evolution will be towards the closure of the hole, even though the flat state is no longer the solution of the originally formulated problem.

Our numerical results [15] indicate that for all  $\alpha \in (0, \pi)$ , there exists a unique value  $\lambda_c \in (-\infty, 0)$  such that  $E(\lambda_c, \alpha) = E_{\text{flat}}$ ; the dependence of  $\lambda_c$  on  $\alpha$  is shown in Fig. 2(b). Furthermore,

$$E(\lambda, \alpha) < E_{\text{flat}} \text{ if } \lambda < \lambda_c, \quad E(\lambda_c, \alpha) = E_{\text{flat}}, \quad E(\lambda, \alpha) > E_{\text{flat}} \text{ if } \lambda_c < \lambda < 0, \quad (3)$$

and moreover, for all  $\alpha \in (0, \pi)$ , there exists a critical volume,  $V_c(\alpha) := V(\lambda_c, \alpha)$ , such that

1.  $E_L < E_{\text{flat}} < E_R$ , if  $0 < V \leq V_c(\alpha)$ ,
2.  $E_{\text{flat}} < E_L < E_R$ , if  $V_c(\alpha) < V < V_{\text{max}}$ ,
3.  $E_{\text{flat}} < E_L = E_R$ , if  $V = V_{\text{max}}$ ,
4. for  $V > V_{\text{max}}$ , there are no steady states, though the *flat configuration* constitutes a possible limiting configuration.

Note that experimental measurement of the mean curvature of the exterior surface of a grain and its spatial variations is typically problematic [14]. Thus, to formulate a criterion which is simpler to verify experimentally, we have defined,  $r_{\text{eff}}$ , the *effective radius* as

$$r_{\text{eff}} := \sqrt{1 - \frac{V}{\pi z(1)}}, \quad (4)$$

where in (4)  $z(1) = z(x = 1)$  denotes the grain height at the wall of the steady state. The effective radius,  $r_{\text{eff}}$ , was seen numerically to depend monotonically on  $\lambda$ . This allowed us to transform the variables  $(\lambda, \alpha) \rightarrow (r_{\text{eff}}, \alpha)$ , which allowed us in particular to uniquely define a *critical effective radius*,  $r_{\text{eff}}^c$ , as  $r_{\text{eff}}^c := r_{\text{eff}}^c(\lambda_c)$ . Surprisingly, we found that  $r_{\text{eff}}^c \approx 0.577$  is independent of the contact angle,  $\alpha$ , making it an even more convenient tool for experimental verification. Thus (3), may be rewritten in terms of  $r_{\text{eff}}^c$  as follows,

$$E(r_{\text{eff}}, \alpha) > E_{\text{flat}} \quad \text{if } r_{\text{eff}} < r_{\text{eff}}^c, \quad E(r_{\text{eff}}^c, \alpha) = E_{\text{flat}}, \quad E(r_{\text{eff}}, \alpha) < E_{\text{flat}} \quad \text{if } r_{\text{eff}} > r_{\text{eff}}^c. \quad (5)$$

See [15] for details. While various definitions of the critical radius have appeared over the years, perhaps most remarkably by Safran & Srolovitz [10], our definition strongly reflects the properties of the steady states and thus yields a quite accurate connection with surface diffusion dynamics, as we shall see shortly. Note that formal evaluation of  $r_{\text{eff}}$  for a flat configuration yields that  $r_{\text{eff}}^{\text{flat}} = 0$ .

### 3.2 Dynamic stability

In this section, we describe the results of our simulations for nodoids, with volume smaller than  $V_c$ . According to the previous section, in this case (see 1.) the left steady state, L, is a global energy minimizer, in particular it has lower energy than any other steady states and less energy than the flat configuration, so it should be linearly as well as non-linearly stable. On the other hand, the right steady state, R, is not even a local energy minimizer, so it cannot be expected to be (linearly or non-linearly) stable. In our dynamic simulations, we found that initial conditions which are a zero-volume perturbation of a right steady state, R, may either converge to its “left” stable partner, L, or evolve until the hole closes, where the basins of attraction for the evolution depends delicately on the time step size in the simulation.

In Figs. 3–5 we show examples of the dynamic evolution of zero volume perturbations of both steady states, R and L, which correspond to  $\alpha = 1$  rad and  $V = 0.328 < V_c$ . In Fig. 3 we portray the evolution of a zero volume perturbation of the stable state, L, where it can be seen that the perturbation diminishes with time until the solution converges to a nodoid, which closely approximates the original unperturbed steady state nodoid. In Fig. 4, we show the evolution of a zero volume perturbation of right steady state R, which converges to its left steady state partner, L, where the time step size is  $\Delta t = 0.01$  and the steady state solution is reached at about time  $T = 1$ . It can be seen that initially the perturbation diminishes and the exterior surface is very close to that of the initial nodoid, then it rapidly shrinks, later slowing down as it approaches steady state. In particular, this simulation visualizes the notion that thin grains tend to shrink faster than thicker grains, whose shape is somewhat reminiscent of hillock formations observed in experiment. Thus, this simulation provides some intuition with regard to various experimentally observed phenomena [5].

In Fig. 5, we show the evolution of a zero volume perturbation of the partner R, which expands until the hole closes. In this simulation  $\Delta t = 1.705 \cdot 10^{-6}$ , and the hole closes approximately at  $T = 1.705 \cdot 10^{-4}$ . Note that initially the evolution is very slow; first the profile of the exterior surface and the mean curvature become monotone increasing functions of  $x$ , and then the contact line speeds up and the velocity of its motion continuously increases as the hole radius decreases.

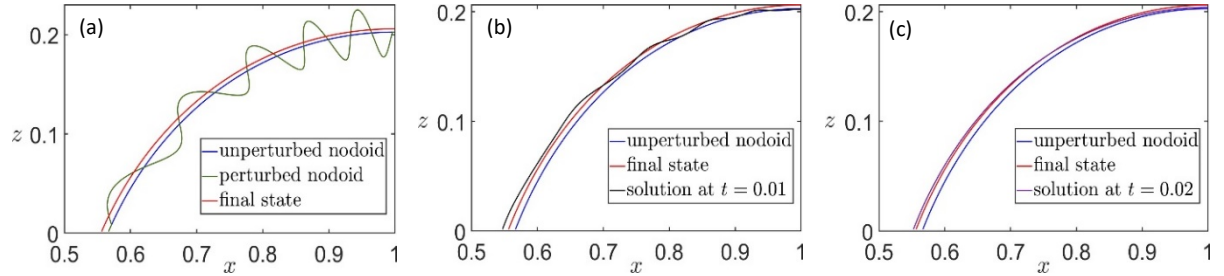


Figure 3: Meridian cross section portrayal of the evolution of a zero volume perturbation of a stable nodoidal steady state, with  $\alpha = 1$  rad and  $\lambda = -0.7$  ( $V \approx 0.328$ ). The blue curve corresponds to the initial steady state, the red curve corresponds to the steady state solution, the green, black, and violet curves correspond to the solution  $z$  versus  $x$  at times:  $t = 0$ ,  $t = 0.01$ , and  $t = 0.02$ , respectively.

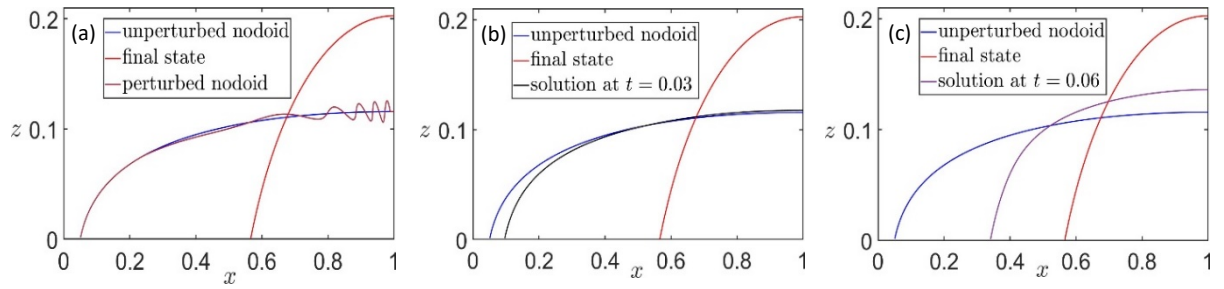


Figure 4: Evolution of a zero volume perturbation of an unstable (nodoidal) steady state (convergence to its more stable “partner,” where  $\Delta t = 0.01$ ), with  $\alpha = 1$  rad and  $\lambda = -0.042$  ( $V \approx 0.32$ ). The blue curve corresponds to the initial nodoid, the red curve corresponds to the steady state solution (obtained at  $T = 1$ ), the maroon, black, and violet curves correspond to the solution  $z$  versus  $x$  at times:  $t = 0$ ,  $t = 0.03$ , and  $t = 0.06$ , respectively.

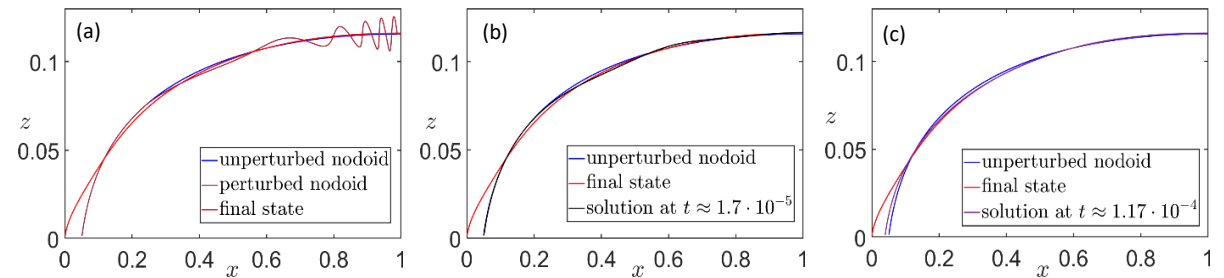


Figure 5: Evolution of a zero volume perturbation of the same unstable nodoidal steady state as in Fig. 4 (with  $\alpha = 1$  rad and  $\lambda = -0.042$ ), but with smaller time steps,  $\Delta t = 1.705 \cdot 10^{-6}$ , which results in the closure of the hole (which occurs for  $T = 1.705 \cdot 10^{-4}$ ). The blue curve corresponds to the initial (unperturbed) nodoidal steady state, the red curve corresponds to the solution just prior the hole closure, the maroon, black, and violet curves correspond to the solution  $z$  versus  $x$  at times:  $t = 0$ ,  $t \approx 1.7 \cdot 10^{-5}$ , and  $t \approx 1.7 \cdot 10^{-4}$ , respectively.

In Fig. 6, we show the evolution of a zero volume perturbation of the R partner in the pair of steady states, with  $\alpha = 1$  rad,  $\lambda = -0.042$ , and with smaller time steps during the simulation,  $\Delta t = 1.705 \cdot 10^{-6}$ . The evolution results in hole closure, accompanied by the formation of a void below the surface. Clearly a limiting configuration without a void would be energetically preferable, and once formed, the void can be locally translated without altering the energy of the system.

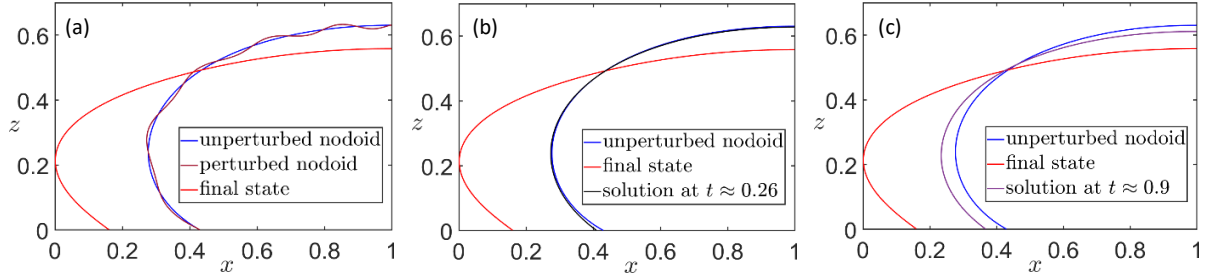


Figure 6: Evolution of a zero volume perturbation of an unstable nodoidal steady state with  $\alpha = 2.5$  rad and  $\lambda = -0.3$ , and with time steps,  $\Delta t = 0.0129$ , which results in the closure of the hole (which occurs for  $T = 1.03465$ ). The blue curve corresponds to the initial (unperturbed) nodoid, the red curve corresponds to the solution just prior the hole closure, the maroon, black, and violet curves correspond to the solution  $z$  versus  $x$  at times:  $t = 0$ ,  $t \approx 0.26$ , and  $t \approx 0.9$ , respectively.

## 4. Conclusions

We have seen that our simple system can mimic many phenomena occurring during wetting and dewetting, including hillock and void formation, as well as hole closure and stable hole formation. We are extending our study of steady states and their energetic and dynamic stability to encompass arguably more realistic systems containing additional grains and holes.

## References

- [1] R. G. W. Brown: *Thin film coatings for optoelectric devices (in Thin Films for Optical Systems)*. Marcel Dekker, New York, 1995.
- [2] C. Delaunay: *Sur la surface de révolution dont la courbure moyenne est constante*. J. Math. Pures Appl. **6**, 309–320, (1841).
- [3] V. Derkach: *Surface and Grain Boundary Evolution in Thin Single- and Poly-crystalline Films*. PhD Thesis, Technion, Haifa, 2016.
- [4] D. Goldberg and A. Novick-Cohen: *Surface diffusion: well-posedness and energetic stability of annular steady states*. in preparation.
- [5] P. Jacquet, R. Podor, J. Ravaux, J. Lautru, J. Teisseire, I. Gozhyk, J. Jupille, and R. Lazzari: *On the solid-state dewetting of polycrystalline thin films: Capillary versus grain growth approach*. Acta Materialia, **143**, 281–290, (2018).
- [6] S. Jahangir, X. Cheng, H. H. Huang, J. Ihlefeld, and V. Nagarajan: *On the solid-state dewetting of polycrystalline thin films: Capillary versus grain growth approach*. J. Appl. Phys., **116**, 163511, (2014).
- [7] C. E. Morosanu: *Thin Films by Chemical Vapor Deposition*. Elsevier, New York, 1990.
- [8] W.W. Mullins: *Theory of thermal grooving*, J. Appl. Phys., **28**, 333–339, (1957).
- [9] E. Shaffir, I. Riess, and W.D. Kaplan: *The mechanism of initial de-wetting and detachment of thin Au films on YSZ*. Acta Materialia, **57**(1), 248–256, (2009).
- [10] D. J. Srolovitz and S. A. Safran: *Capillary instabilities in thin films. I Energetics*. J. Appl. Phys., **60**(1), 247–254, (1986).
- [11] D. J. Srolovitz and S. A. Safran: *Capillary instabilities in thin films. II Kinetics*. J. Appl. Phys., **60**(1), 255–260, (1986).

- [12] H. Wong, M. J. Miksis, P. W. Voorhees, and S. H. Davis: *Capillarity driven motion of solid film wedges*. *Acta Mater.*, **45**(6), 2477–2484, (1997).
- [13] H. Wong, P. W. W. Voorhees, M. J. Miksis, and S. H. Davis: *Capillary instabilities of a catenoidal hole in a solid film*. *J. Appl. Phys.*, **81**(9), 6091–6099, (1997).
- [14] X. Zhong, M. N. Kelly, H. M. Miller, S. J. Dillon, and G. S. Rohrer: *Grain boundary curvatures in polycrystalline SrTiO<sub>3</sub>: Dependence on grain size, topology, and crystallography*. *J. Am. Ceram. Soc.*, **102**, 7003–7014, (2019).
- [15] A. Zigelman and A. Novick-Cohen: *Critical effective radius for holes in thin films. Energetic and dynamic considerations*. *J. Appl. Phys.*, **130**, 175301, (2021).